

Developments in *MAT_WINFRITH_CONCRETE and Application to Modelling of Segmented Concrete Tunnel Linings

Richard Sturt¹, Gianmarco Montalbini¹, Hyuk-II Jung¹, Marc Tatarsky²

¹Arup, UK ²Arup, USA

1 Abstract

Tunnels constructed by Tunnel Boring Machines are lined with precast reinforced concrete segments. The joints between the segments must resist a combination of compressive load and bending moments induced by non-uniform pressure from the soil. Failure modes to be considered during design include splitting of the joint face under concentrated compressive load, spalling of the exterior or interior faces of the segments under bending actions, and impacts of bolt connection details on the stability of the joints. The capacity of the segments to resist such failures may be explored in detail using LS-DYNA's nonlinear concrete models. The paper includes examples from an investigation into a tunnel that partially collapsed shortly after construction. The failure modes revealed by the site investigation of the collapsed tunnel matched well with those shown by the model.

The models described in this paper make use of some enhancements to the "Winfrith" concrete material model (*MAT_084) that will be released in R15, such as confinement-dependent post-yield softening in compression, which is applicable to all types of concrete, and post-cracking softening controlled by a user-supplied curve which is particularly applicable to steel fibre reinforced concrete (SFRC). These enhancements are described in detail in the first half of the paper. The material model is now capable of simulating all the likely failure modes of tunnel segment joints including spalling, bearing and shear failures as well as splitting of the joint face.

2 Introduction

This paper covers two overlapping subject areas. Firstly, a number of developments in *MAT_WINFRITH_CONCRETE (*MAT_084) will be described. These are applicable to modelling static and quasi-static loading of any concrete structure, including (but not limited to) tunnel linings. Secondly, applications to tunnel linings made from conventional reinforced concrete and from steel fibre reinforced concrete (SFRC) are discussed.

*MAT_WINFRITH_CONCRETE was developed by Broadhouse and Neilson in the 1980s [1],[2]. The original implementation is available by setting the input parameter RATE to 0 or 1 (where these values invoke strain-rate-sensitive or non-strain-rate-sensitive algorithms respectively). In LS-DYNA R9, a new setting of RATE=2 was introduced which invoked certain improvements in the cracking algorithm.

One of the strengths of the model has always been its ability to develop realistic cracks that can be observed and displayed in the results. On the other hand, a serious shortcoming was the unrealistic perfectly-plastic post-yield response in compression, whereas real concrete softens rapidly, especially if unconfined. This has limited the applicability of MAT_084 to situations in which tensile failure (cracking) was the governing behaviour to be modelled. Furthermore, steel fibre reinforced concrete (SFRC) could not be modelled due to the lack of an option for user-defined post-cracking tensile behaviour.

The objectives of the developments described in this paper are to extend the applicability of MAT_084 to include simulation of other failure modes that are potentially important in structural engineering (such as compressive/bearing and shear failures) while retaining the existing strengths in modelling cracking, and extending its applicability to SFRC. The new developments are accessed by setting RATE to 8 and herein will be referred to for brevity as "RATE=8". RATE=8 includes the improved cracking algorithm of RATE=2 together with a range of features that address the previous limitations and provide additional capability. It is applicable to static and quasi-static loading of all types of concrete structures, but because it does not offer strain-rate sensitivity, it is less suitable for modelling dynamic loading such as blast or impact. RATE=8 will be available starting from LS-DYNA R15.

The paper does not cover comparisons with other LS-DYNA material models for concrete such as MAT_072R3, MAT_159 (CSCM) or MAT_273; this would be a useful topic for future publications.

Tunnels constructed by Tunnel Boring Machines (TBMs) are lined with precast concrete segments that are placed by the TBM and may then be bolted together in a subsequent manual operation. The faces of the segments that bear against each other are termed “joints”. Structurally, the job of the segments is to resist external pressure from the soil which results in compressive circumferential loading of the lining. Furthermore, the soil stress applied horizontally at axis level usually differs from the soil stress applied vertically at the crown and invert of the tunnel, resulting in bending moments in the lining and a tendency to ovalise. Joint faces need to be designed to resist these forces. This may be done via conventional reinforcement and/or by mixing steel fibres into the concrete. The latter approach adds cost, but offers advantages in terms of additional resistance to damage to the segment edges and corners during handling prior to installation. A segment design based purely on SFRC without conventional reinforcement bars may also offer a faster cycle time for mass-production.

It is desirable to validate segment designs by laboratory testing, but given the cost and timescales involved, there is value in prior assessment and design optimization using nonlinear analysis. These would include serviceability and ultimate load assessments, requiring the capability to model responses from the development of small cracks through to ultimate failure.

3 Developments in *MAT_WINFRITH_CONCRETE

This section describes some of the principal features of RATE=8 which make it different from previously-available versions of MAT_084. Space does not permit a complete description, but further information will be given in the user manual.

3.1 Yield surfaces

The strength of concrete under multiaxial stress states has been extensively researched experimentally and numerous analytical expressions for the yield surface have been devised to fit the experimental results. The yield surface by Ottosen [3] is a commonly adopted choice. It is the one adopted in all implementations of *MAT_084 and is also recommended for analysis of concrete under multiaxial stress states in fib Model Code for Concrete Structures 2010 [4] (hereafter abbreviated to MC2010), a widely-used reference for all aspects of the behaviour of concrete. The Ottosen yield surface is defined as follows:

$$\alpha \frac{J_2}{\sigma_c^2} + \lambda \frac{\sqrt{J_2}}{\sigma_c} + \beta \frac{I_1}{\sigma_c} - 1 = 0 ,$$

where

$$\lambda = c_1 \cos \left[\frac{1}{3} \arccos(c_2 \cos(3\theta)) \right] .$$

In the above I_1 , J_2 and J_3 are the first, second and third stress invariants, σ_c is the uniaxial compressive strength, and θ is the Lode Angle. α , β , c_1 , and c_2 are calibration constants that are calculated such that the yield surface passes through four reference stress states. Two of the reference states are uniaxial compression and uniaxial tension (in MAT_084 these stresses are given by the input parameters UCS and UTS respectively), but different authors have recommended different procedures for determining the other two reference stress states through which the yield surface must pass. Therefore, although the Ottosen yield surface equation remains the same, the values of the calibration constants (and hence the exact shape of the yield surface) differ between different implementations. In this respect, the procedure adopted by Broadhouse and Neilsen (which is hard-wired in the original MAT_084 implementation) differs from the procedure set out in MC2010. The default for RATE=8 is to follow MC2010 (controllable via the input parameter OTTO). In both cases the reference stress states and the constants are calculated automatically using UCS and UTS as inputs. The difference obtained from the two approaches is illustrated by the curves labelled 1 and 2 in Fig.1, which shows intersections of the yield surfaces with the plane $\sigma_3=0$ (plane stress). Annotated on the graph as A, B and C are three of the reference stress states (the fourth is a “triaxial” point that does not lie on the plane depicted in the graph).

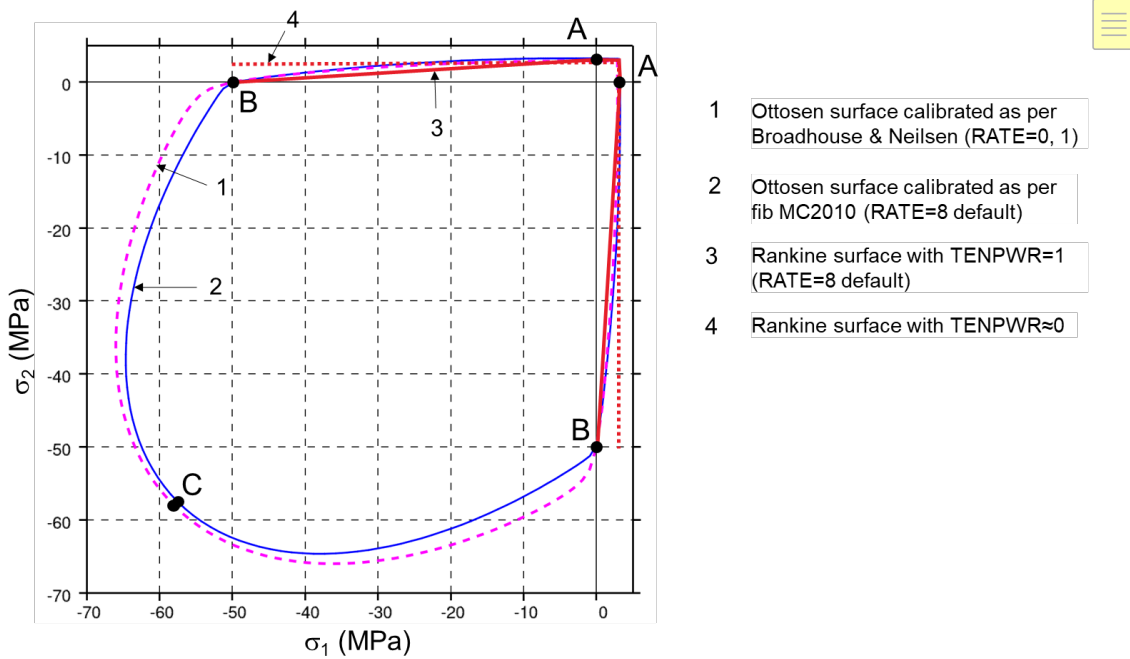


Fig.1: MAT_084 yield surfaces.

3.1.1 Tensile failure

Although the Ottosen yield surface was originally devised to cover both compressive and tensile failure, the post-failure behaviour of concrete differs greatly between these two stress states. Furthermore, tensile cracking has little influence on the subsequent ability of the material to carry compression. For these reasons, it has been found necessary to introduce a separate yield and failure treatment for tension, leaving the Ottosen surface to cater for compressive failures.

The RATE=8 implementation considers tensile failure via a Rankine surface, which defines the (tensile) principal stress at which a crack is initiated. If all of the principal stresses are tensile or zero, then the tensile strength is equal to UTS (top-right quadrant of Fig.1). If compressive stresses are also present, then the tensile strength depends on the input parameters TENPWR and TENRSD. The default setting of TENPWR is 1.0, giving the solid red line labelled 3 in Fig.1. This setting ensures that, as the stress increases from zero along any stress path containing at least one tensile principal stress, the Rankine surface will be reached before the Ottosen surface and therefore the cracking algorithm will be invoked. In contrast, if TENPWR were set at a low value (obtaining the dotted red line labelled 4 in Fig.1), some stress paths would reach the Ottosen surface first resulting in yielding rather than cracking. Note also that, because of the action of TENPWR, the tensile strength of any given element (denoted f_t herein) may differ from the input value UTS.

3.1.2 Influence of tensile strength on Ottosen yield surface

An unexpected implication of the method of calibrating the Ottosen yield surface (which applies to both the Broadhouse & Neilsen and the MC2010 procedures) is that the input value for tensile strength (UTS) impacts on the shape of the whole Ottosen yield surface, including in the regions where all three principal stresses are compressive. For this reason, it is important to input a realistic tensile strength for UTS, and not a low “design” value. This is illustrated in Fig.2, in which the solid line is the yield surface created when realistic input values are given for UCS and UTS of 50 and 2.9 MPa respectively, while the dotted line gives the yield surface obtained when UTS is reduced to 0.5 MPa. Note the extreme effect on the curve in the region $-10 < \sigma_2 < 0$ which would imply an unrealistically high compressive strength in the presence of a small compressive confining stress.

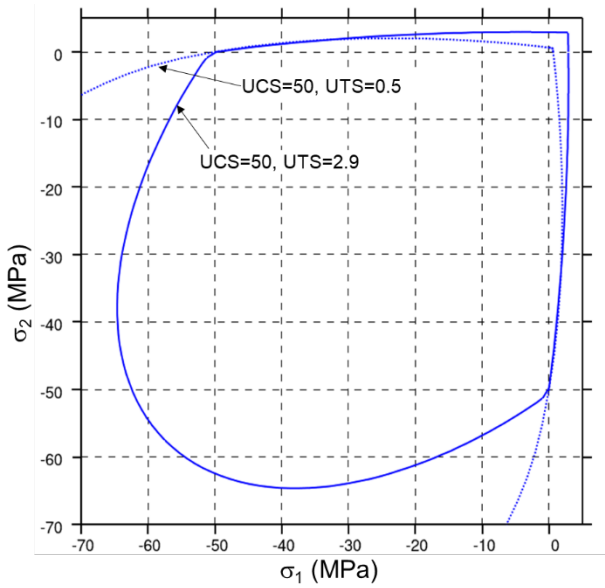


Fig.2: Influence on Ottosen yield surface of artificially-low input value of tensile strength

During design, however, it is often desired to check that the performance of a structure is not reliant on the tensile strength of concrete, which may in practice be reduced by cracking due to shrinkage or other reasons. To accommodate this, RATE=8 provides a facility for scaling down the tensile strength as a function of time: input curve LCFTIM, the ordinate of which is a scaling factor applied to UTS. The Ottosen yield surface calibration is done at initialization only. A realistic value is input for UTS, together with a curve LCFTIM that starts with an ordinate of 1.0 ensuring a suitable Ottosen yield surface. The curve can then drop to a lower value (shown conceptually in Fig.3) enabling cracks to form in response to tensile stresses less than UTS.

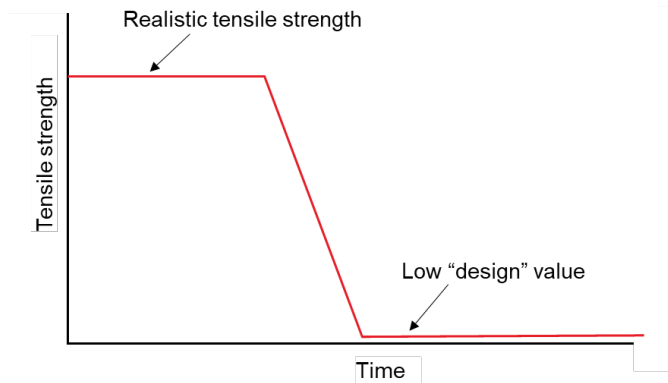


Fig.3: Use of input curve LCFTIM to apply low “design” value of tensile strength

3.2 Post-yield behaviour: general approach

Up to three mutually-perpendicular cracks are allowed, denoted with subscripts *crack1*, *crack2*, and *crack3* below. A smeared crack algorithm is used, i.e. the presence of the crack is modelled by modifications to the stress-strain behaviour, rather than by the mesh splitting apart. Cracking is considered separately from yielding on the Ottosen yield surface, denoted with subscript *p* below. In all, the total strain increment tensor, $d\boldsymbol{\varepsilon}_{total}$, potentially consists of five tensor components:

$$d\boldsymbol{\varepsilon}_{total} = d\boldsymbol{\varepsilon}_{elastic} + d\boldsymbol{\varepsilon}_p + d\boldsymbol{\varepsilon}_{crack1} + d\boldsymbol{\varepsilon}_{crack2} + d\boldsymbol{\varepsilon}_{crack3}$$

The displacement of each crack, δ_{crack} , is calculated by summing the incremental crack strains and scaling by element size, which is approximated from the element’s initial volume, Vol_0 :

$$\delta_{crack} = Vol_0^{1/3} \sum d\varepsilon_{crack}$$

Crack-opening displacements are tracked such that if the crack fully closes later in the calculation, compressive stress can be carried. Cracks are treated as non-rotating, meaning that, after the crack has formed, its orientation relative to the element axes remains unchanged. This, together with the limitation of no more than three mutually-perpendicular cracks, can lead to tensile stresses greater than the input tensile strength UTS being observed in results if the loading direction rotates after formation of the first crack.

3.3 Post-yield stress-strain behaviour in tension

After formation of a crack, application of further tensile strain causes the crack to open and the tensile stress to reduce. The stress reduction is modelled as a function of crack-opening displacement rather than strain, in order to reduce sensitivity of results to mesh size. In the original RATE=1 implementation, the function is a linear reduction of tensile stress to zero at a crack opening displacement equal to the user-specified input parameter FE. This is also the default for RATE=8, but a user-defined curve may be input instead. The latter is needed for fibre-reinforced concrete, in which opening of the crack continues to be resisted by yielding or pull-out of the fibres after the concrete itself has lost all tensile capacity, as illustrated conceptually in Fig.4.

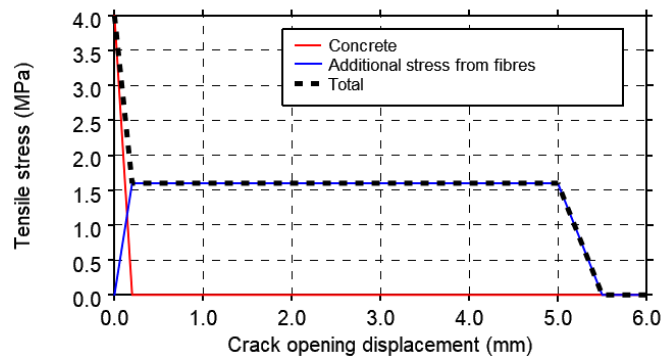


Fig.4: Example of tensile stress-strain input data for Steel Fibre Reinforced Concrete (SFRC)

3.4 Crack propagation

After initiation of a crack, its propagation through a structural member is facilitated by stress concentrations around the crack tip, which are on a smaller geometric scale than can be captured by typical finite element meshes. A crude representation of this effect is available in RATE=8 whereby, once an element cracks, the tensile strength of uncracked neighbouring elements is reduced in a manner similar to the “crush front” in some material models for composites such as MAT_054. Fig.5 shows an example of neighbouring elements around a crack.

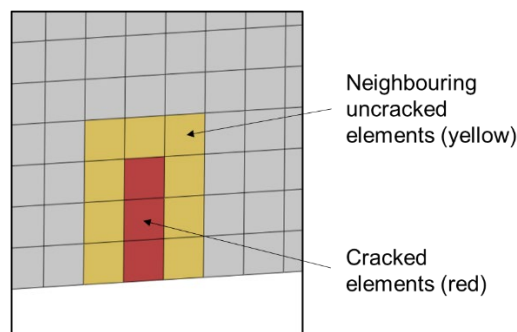


Fig.5: Elements with reduced tensile strength next to a crack

The reduced tensile strength of the neighbour elements, f'_t , is controlled by input parameters CRFAC and COD1 as follows:

$$f'_t = f_t \left[1 - CRFAC \left(\min \left(1.0, \frac{\delta_{crack,max}}{COD1} \right) \right) \right]$$

In the above, f_t is the undamaged tensile strength and $\delta_{crack,max}$ is the maximum crack opening displacement of any neighbouring cracked elements. The parameter COD1 provides a smooth transition between undamaged and damaged conditions. Note that f'_t is not necessarily equal to UTS, as explained in 3.1.1.

An obvious shortcoming of this approach is that all neighbouring elements are weakened, rather than only the ones that are directly in line with the crack – in reality, it is the latter that would be most affected by the concentrated tensile stress at the tip of the crack.

3.5 Shear transfer across cracks

As well as crack-opening, i.e. direct strains normal to the crack plane, the crack strain tensor $d\epsilon_{crack}$ may include shear components which represent the crack surfaces sliding over each other. The surfaces of cracks in concrete are not smooth and typically pass around particles of aggregate. Resistance to sliding, known as “aggregate interlock”, is modelled in RATE=8 with equations from Vecchio and Collins [5]. The equations, which calculate the maximum shear stress across a crack, τ_{max} , cater for situations in which the crack is open with displacement δ_{crack} , or closed with compressive stress σ_c . In the “neutral state”, where the crack is closed but has no compression acting on it, the maximum shear stress on the crack is equal to 1.16 times the tensile strength of the concrete.

$$\tau_{max} = 0.18\tau_{rm} + 1.64\sigma_c - 0.82 \frac{\sigma_c^2}{\tau_{rm}}$$

$$\tau_{rm} = \frac{2f_t}{0.31 + \frac{24\delta_{crack}}{(D_0 + 16)}}$$

In the above, D_0 is the aggregate size in millimetres and f_t is the initial tensile strength of the concrete. In LS-DYNA, for purposes of the aggregate interlock calculation, f_t is by default equal to UTS but can be overridden with the input parameter FTSHR if desired.

The action of the above equations may be seen in the example in Fig.6 for concrete with tensile strength 3.0MPa.

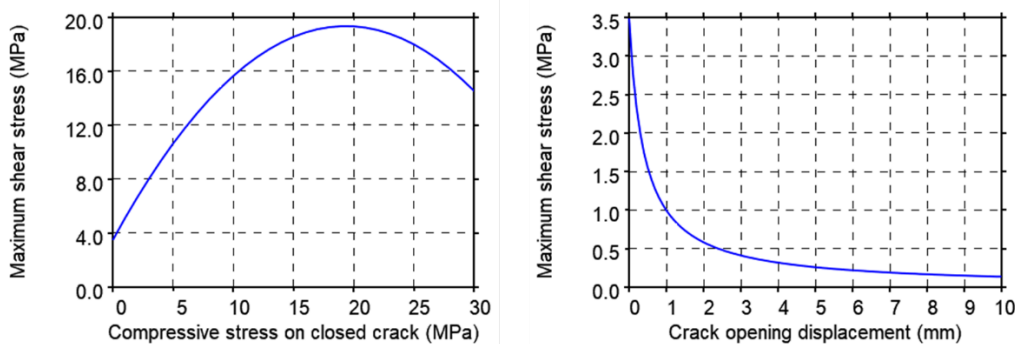


Fig.6: Maximum shear stress that can be carried across a crack

3.6 Post-yield behaviour in compression

3.6.1 Uniaxial stress conditions

The perfectly-plastic post-yield behaviour in compression is one of the principal limitations of the original implementation of MAT_084. RATE=8 offers a user-defined curve (LCCMP) to control post-yield softening as a function of the plastic strain associated with yielding on the Ottosen surface. The ordinate of the curve is a non-dimensional scale factor applied to the compressive strength. Under uniaxial

compressive stress conditions, the initial compressive strength is equal to the input parameter UCS, and the post-yield stress, $\sigma_{Y,uniaxial}$, varies with plastic strain, $\varepsilon_{p,uniaxial}$, as follows:

$$\sigma_{Y,uniaxial} = LCCMP(\varepsilon_{p,uniaxial}) \cdot UCS$$

This is achieved by replacing σ_c in the Ottosen yield function with $\sigma_{Y,uniaxial}$. The significance of the subscript “uniaxial” applied to the plastic strain in the above equation will be made clear later. An example stress-strain response for uniaxial stress conditions is given in Fig.7, comparing RATE=1 with RATE=8.

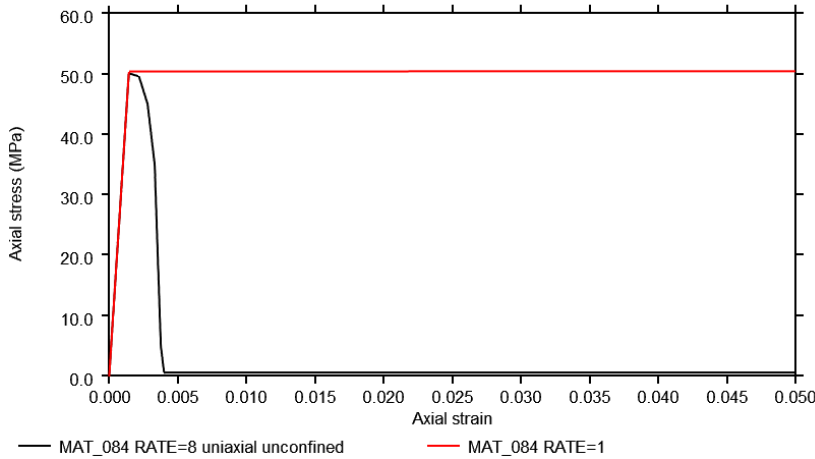


Fig.7: Uniaxial stress-strain response in compression, RATE=1 (red) and RATE=8 (black)

3.6.2 Multiaxial conditions: influence of confining stresses on compression response

Confined conditions occur in reinforced concrete structures when the reinforcement cage resists expansion of the concrete in the directions perpendicular to the main compressive load. Under these conditions, the stress state in the concrete consists of one large compressive stress in the loading direction and, typically, two smaller compressive stresses (“confining stresses”) in the perpendicular directions. The influence of the confining stresses is twofold: firstly, the compressive strength in the loading direction is increased from the uniaxial value to an enhanced value (often denoted in the literature as f_c and f_{cc} respectively); and secondly, the compressive response becomes more ductile, meaning that the rate of softening with strain is reduced and the strain to failure is increased. The increase of strength is modelled in MAT_084 by the Ottosen yield surface for all settings of RATE. The increase of ductility is accounted for in the RATE=8 implementation by a feature controlled by input parameter CDSF that has the effect of stretching the user-supplied softening curve LCCMP along the strain axis as a function of the strength enhancement factor f_{cc}/f_c . Recognising that confinement conditions may change with time, the ductility enhancement is applied incrementally to calculate the uniaxial-equivalent plastic strain, $\varepsilon_{p,uniaxial}$, which is smaller than the sum of the actual plastic strain increments $d\varepsilon_p$. It is $\varepsilon_{p,uniaxial}$ which is then used as the abscissa of curve LCCMP as noted in 3.6.1.

$$\varepsilon_{p,uniaxial} = \sum \left[\frac{d\varepsilon_p}{1 + CDSF(f_{cc}/f_c - 1)} \right]$$

The action of CDSF on the compressive stress-strain curve is illustrated in Fig.8. It applies a “stretch factor” along the strain axis that has a linear relationship with the enhancement of compressive strength resulting from the confinement conditions. CDSF has no effect on the uniaxial stress (unconfined) response because f_{cc} is then equal to f_c . A default value of CDSF=13 is provided with RATE=8, but the appropriate value may vary for different strengths and types of concrete and users may wish to calibrate this parameter against test data or analytical expressions in the literature.

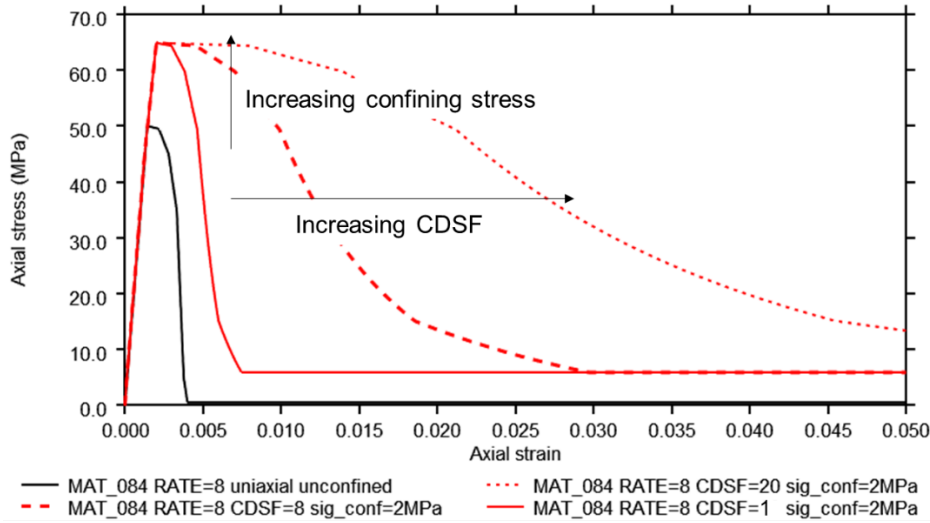


Fig.8: Influence of CDSF on compression response under 2 MPa confining stress (red curves) and unconfined response (black curve)

Example stress-strain responses are shown in Fig.9 for concrete with 50MPa uniaxial compressive strength under confining stresses of 0, 2 and 4MPa, with CDSF set to 8. Comparisons are provided with analytical curves by Montoya et al [6] that were derived from experimental results. While the post-peak response matches the analytical curves well, the lack of pre-peak nonlinearity remains a limitation. An alternative analytical expression by Mander et al [7] can be used to construct stress-strain curves similar to those in the Figure below; a setting of CDSF=13 was found to provide a reasonable match to the Mander curves in the post-peak regime.

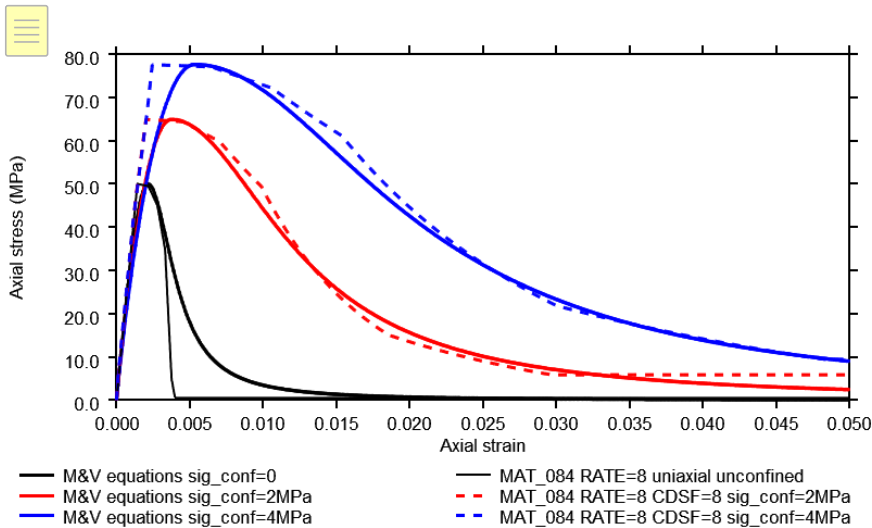


Fig.9: Stress-strain curves under compressive loading compared with analytical expression by Montoya et al

3.7 Outputs

The “extra history variables” that may be output from RATE=8 differ from those from RATE=0 and 1. Of particular interest during post-processing are the crack opening displacements (δ_{crack1} , δ_{crack2} and δ_{crack3}) and the plastic strain due to yielding (ϵ_p). The crack opening displacements are output in model length units. They are intended to correspond to crack widths measured in real-life structures, although in reinforced concrete the spacing between cracks (and hence the width of each crack) may be

influenced by the properties of the bond between concrete and reinforcement bars so accurate prediction of crack widths can depend on accurate modelling of the bond.

For RATE=8, the variable written to the d3plot file in place of plastic strain combines cracking and yielding into a single measure of damage with length units, δ_{dam} , defined as follows:

$$\delta_{dam} = \varepsilon_p Vol_0^{1/3} + \delta_{crack1} + \delta_{crack2} + \delta_{crack3}$$

This is the variable displayed in the contour plots in the Figures in Sections 4 and 5.

4 Calibration

4.1 Calibration of compression response

The compressive strength of concrete is measured using standard cylinder and/or cube tests. Cylinders are typically 150mm diameter and 300mm high (and always in a 1:2 aspect ratio), while cubes are typically 150mm side length, although EN 12390-1 [8] does permit a range of other sizes. The uniaxial compressive strength is by definition equal to the maximum stress developed in a cylinder test, where “stress” means the nominal stress calculated from the load divided by the initial cross-sectional area. Cubes typically develop a maximum nominal stress that is 15-25% greater than cylinders, because the lower aspect ratio of the cube results in greater influence of the confinement effect caused by friction on the loading plattens. As an example, Eurocode 2 [10] gives the characteristic cylinder and cube strengths of a C50 grade concrete as 50MPa and 60MPa respectively.

Typical results from simulations of cylinder and cube tests using MAT_084 with RATE=8 are shown in Fig.10. The uniaxial compressive strength of the concrete in this case is 50MPa. A friction coefficient of 0.5 is defined on the loading plattens. In practice, cylinder test models usually fail at a stress very close to the uniaxial compressive strength (input parameter UCS) so they do not give rise to any requirement for calibration of the material input data. Cube test simulation results, on the other hand, are sensitive to the strain-softening curve LCCMP, which can be calibrated such that the expected cube test strength is achieved.

4.2 Calibration of tensile response

Direct tensile tests are difficult to perform on concrete. More commonly, tensile strength is estimated from splitting tests as defined in EN 12390-6 [9] in which a cylinder of concrete is compressed across its diameter. The tensile strength of the concrete, f_t , is then calculated from the maximum load, F , using the following equation:

$$f_t = \frac{2F}{\pi DL}$$

In the above, D and L are the cylinder diameter and length respectively. The splitting test can be simulated with MAT_084 as illustrated in Fig.10, typically giving a result for f_t that is close to the input parameter UTS; after setting UTS= f_t , further calibration is not usually required. Where the tensile strength of a particular concrete is unknown, it can be taken from the properties of the appropriate grade of concrete given in standards such as Eurocode 2.

4.3 Validation of shear failure

Tests were performed by Wong et al [11], in which a concrete specimen 140x140x300mm was grouted into two metal boxes, leaving a 20mm high “shear band” between the upper and lower boxes. The lower box was held fixed, a constant compressive vertical load was applied, then the upper box was displaced horizontally as shown in Fig.11. The experiment was repeated with vertical loads of 3.0, 4.4 and 6.0 MPa. The same concrete mix was subjected to uniaxial compression and splitting tests, yielding a compressive strength of 41 MPa and a tensile strength of 4.9 MPa (median of three tests). The experiment was modelled using MAT_084 RATE=8 with a 5mm mesh size. Other than inputting these values as UCS and UTS, no further adjustment or calibration of input properties was carried out. Maximum shear stresses from the model are compared with the test results in Fig.11. Given that only three experiments were performed, and some test-to-test variability is expected, the correlation obtained is considered satisfactory.

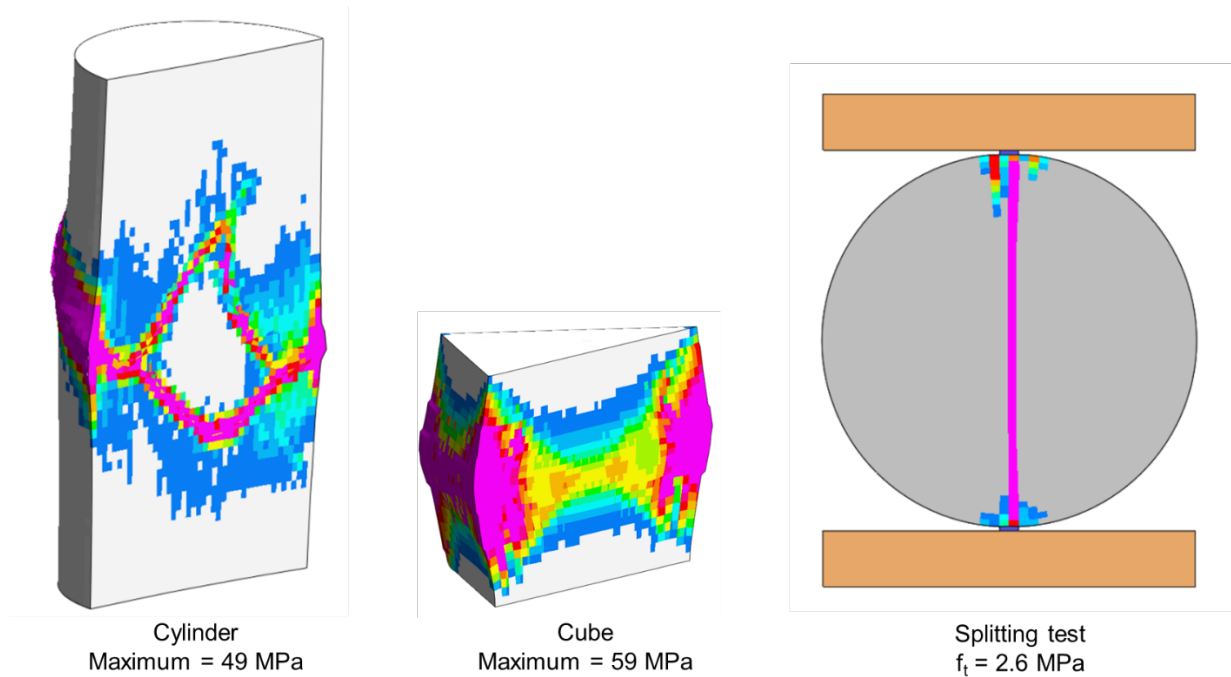


Fig.10: Simulations of calibration tests, MAT_084 RATE=8 with UCS=50MPa, UTS = 2.9MPa

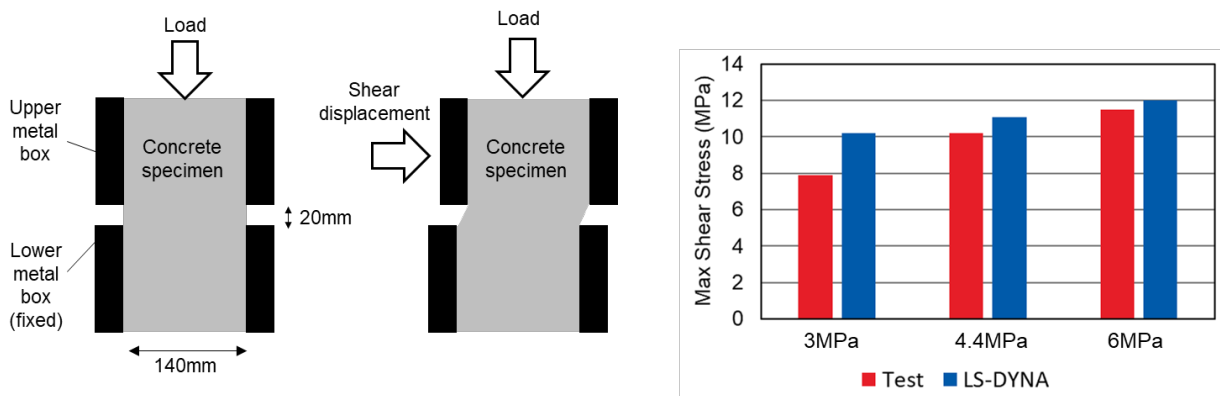


Fig.11: Shear box test from Wong et al [11] and results from MAT_084 for Load = 3.0, 4.4 and 6.0 MPa.

4.4 Split beam test for Steel Fibre Reinforced Concrete

Tensile behaviour of SFRC is quantified by a three-point bending test on a beam containing a notch on the tension side, for example as defined in EN 14651 [12]. The notch initiates a crack in the concrete which propagates towards the top surface of the beam. Opening of the crack is resisted by the steel fibres. The “residual flexural tensile strength”, f_R (in stress units) is back-calculated from the force measured at the point of load application, F , using the following equation:

$$f_R = \frac{3Fl}{2bh_{sp}^2}$$

where l is the beam span length, b is the width of the specimen, and h_{sp} is the depth of the specimen from the tip of the notch to the top surface.

The increase of width of the notch, described as the Crack Mouth Opening Displacement (CMOD), is also measured. The output of the test consists of the values of f_R at peak resistance (known as Limit of Proportionality or LOP) and at CMOD values of 0.5, 1.5, 2.5 and 3.5mm, described as f_{R1} , f_{R2} , f_{R3} and f_{R4} respectively. An LS-DYNA model of the notched beam can be calibrated by adjusting the tensile stress-strain curve such that these residual flexural tensile strengths match the measured or specified values, as shown in the example in Fig.12.

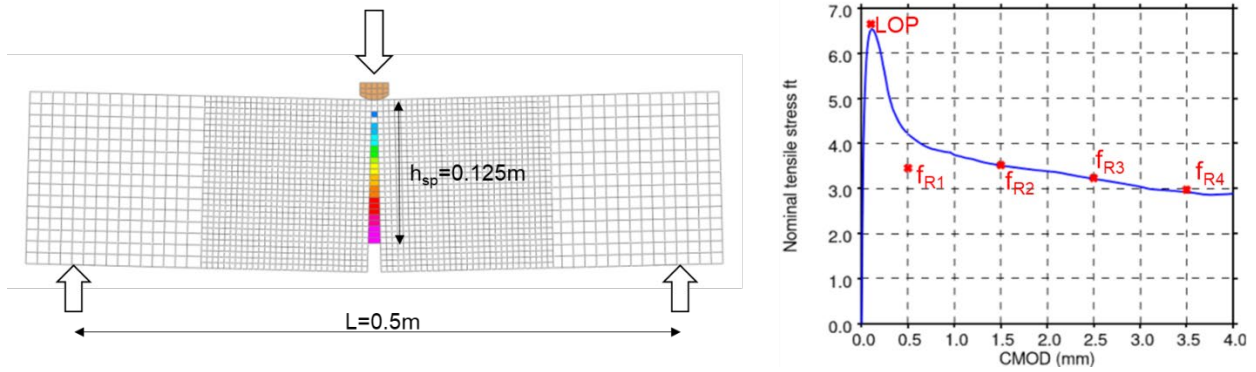


Fig.12: Simulation of notched beam test. Contour colours show crack width. Graph shows simulation (blue) and test (red).

5 Applications

5.1 Punching shear

A test case modelling punching shear is illustrated in Fig.13. The model consists of part of a 5.5m thick reinforced concrete transfer structure. The reinforcement bars are modelled explicitly with beam elements; these are fixed to the concrete using *CONSTRAINED_BEAM_IN_SOLID. In this test case, a square rigid pusher applies load to the top surface, while the underside is supported by a square-shaped rigid frame leaving a 16m clear span in each direction.

The predicted failure mode consists of a cone-shaped region of shear deformation and cracks together with a central vertical crack (splitting), which is as expected. Shear failure in reinforced concrete is typically considered using strut-and-tie methods, in which the reinforcement bars (including the vertical shear links) work in tension while the concrete provides a diagonal compression “strut”. Hand calculations based on this principle following the method in AASHTO LFRD [13] yielded a design value ultimate load of 460MN, while LS-DYNA predicted an ultimate load of 610MN. The hand-calculation is expected to be on the conservative side.

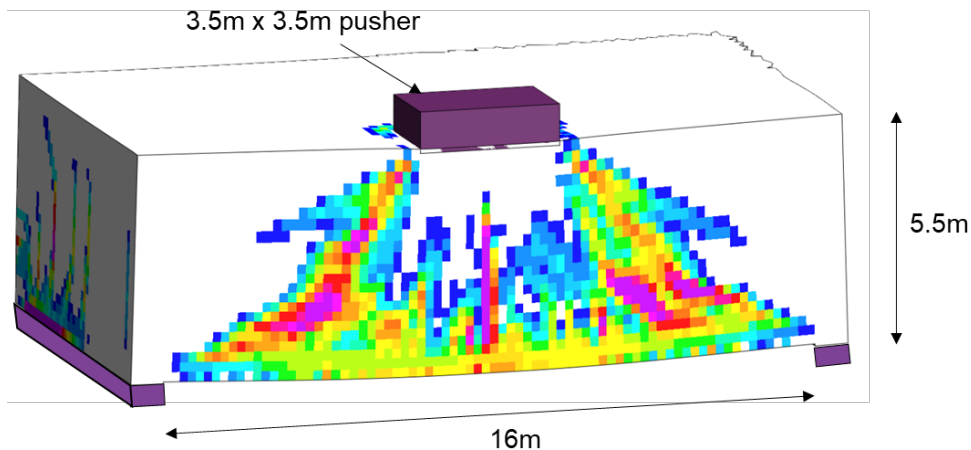


Fig.13: Simulation of punching shear failure of 5.5m thick transfer structure. Displacements shown magnified.

5.2 Investigation into the collapse of a tunnel

The tunnel described in this example was constructed by Tunnel Boring Machine (TBM) with a lining consisting of conventionally reinforced precast concrete segments. The general layout and terminology used to describe the joints are illustrated in the left-hand image of Fig.14.

The stability of segmented tunnel linings depends primarily on circumferential compression generated by external pressure from the soil, although bolts are provided as well. In this case, unexpected events occurred in the soil outside the tunnel which reduced the external pressure on the sides of the tunnel to

the point that several tens of metres of the tunnel collapsed. The collapsed section has been excavated, revealing the post-failure condition of the segments. During the collapse event, the joints were subjected to deformations far in excess of their normal design range. As such, this example provides an unusual opportunity for observing the ultimate failure modes of precast tunnel segments. The right-hand image of Fig.14 shows the deformation mechanism. Different joints are subjected to different loading conditions, annotated A, B and C in Fig.14.

- A: Near the top (“crown”) and bottom (“invert”), radial joints are rotated such that a gap opens at the inner surface (“intrados”) while compressive load is concentrated at the outer surface (“extrados”);
- B: Near the sides, the opposite situation occurs (“extrados-opening” of radial joints);
- C: The circle joints are loaded in shear due to incompatibility of deformation mode between one ring of segments and the next.

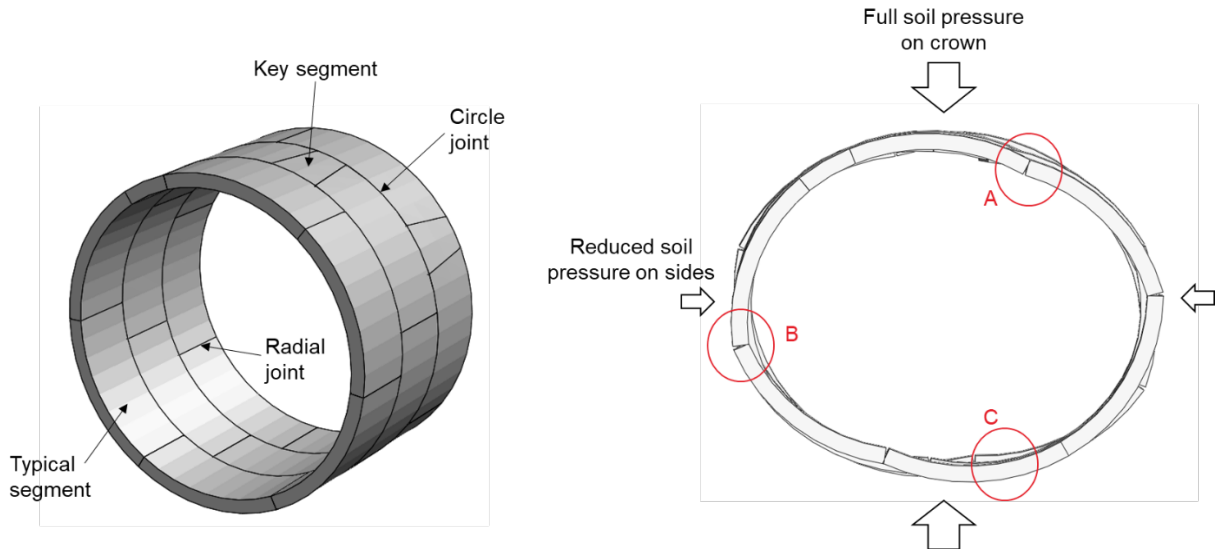


Fig.14: Left: Terminology used in descriptions of joints. Right: Deformation mechanism (magnified displacements).

One radial joint and one circle joint were modelled in detail with LS-DYNA using *MAT_084 with RATE=8. The objectives of the work, which relate to a larger exercise supporting the recovery and strengthening of the tunnel, will not be described here. Instead, a selection of results from these models will be presented and compared against site observations.

The extents of the detailed models representing the two joint types are shown in Fig.15, and the models are shown in more detail in Fig.16. The mesh size is around 5mm near the joint faces. As well as the concrete segments themselves, the models include reinforcing bars, bolts and sealing gaskets. All these are modelled with solid elements except the reinforcing bars which are modelled with beam elements (drawn with their true section sizes in Fig.16).

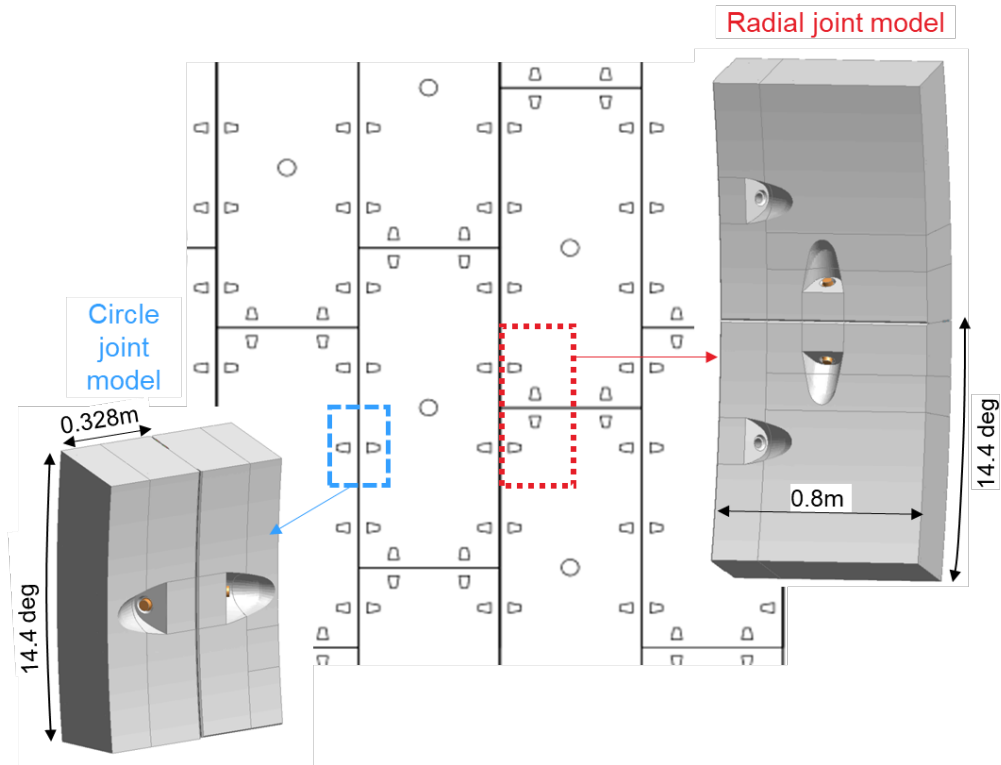


Fig. 15: Extents of LS-DYNA tunnel segment joint models

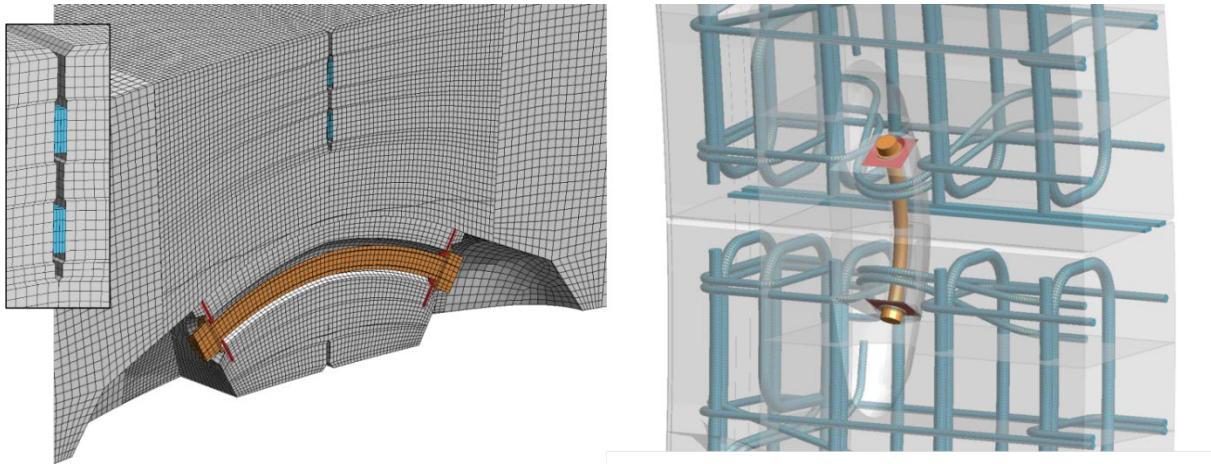


Fig. 16: Segment model details

The models were subjected to a staged application of loading that reflects the sequence of construction followed by displacement in a given direction representing events occurring during the collapse, as indicated in Fig. 17 for the example of intrados-opening rotation applied to the radial joint. The models were run separately for different loading directions including rotation in both directions for the radial joints, and shear displacements in two directions for both types of joint.

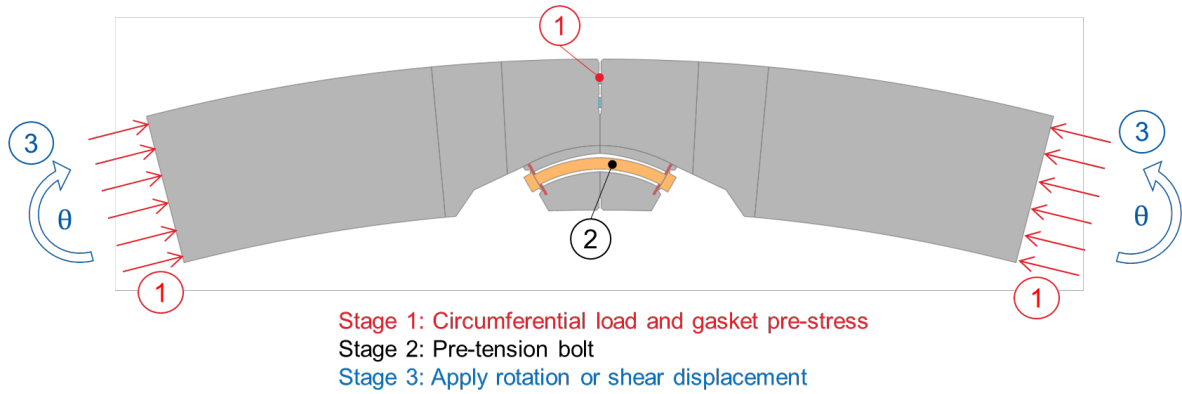


Fig.17: Segment model loading sequence

Example results are given in Fig.18, Fig.19 and Fig.20. The bending and shear loads at which the observed joint failures occurred cannot be known, and nor has it been possible to carry out laboratory testing on these segments, so the models cannot be correlated quantitatively with reality; however, the failure modes in the finite element models seem plausibly similar to the site observations.

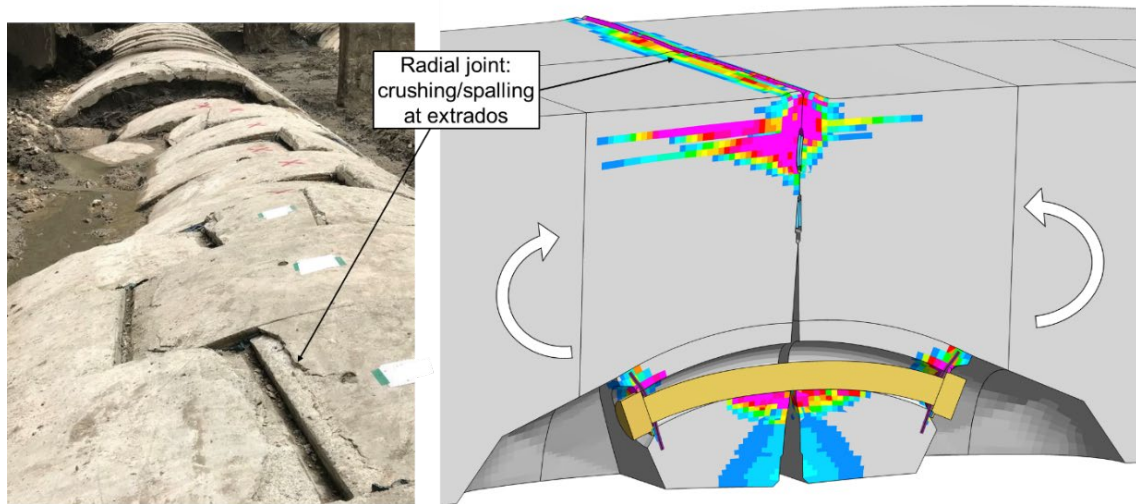


Fig.18: Simulation of intrados-opening rotation of radial joint compared with excavated segments

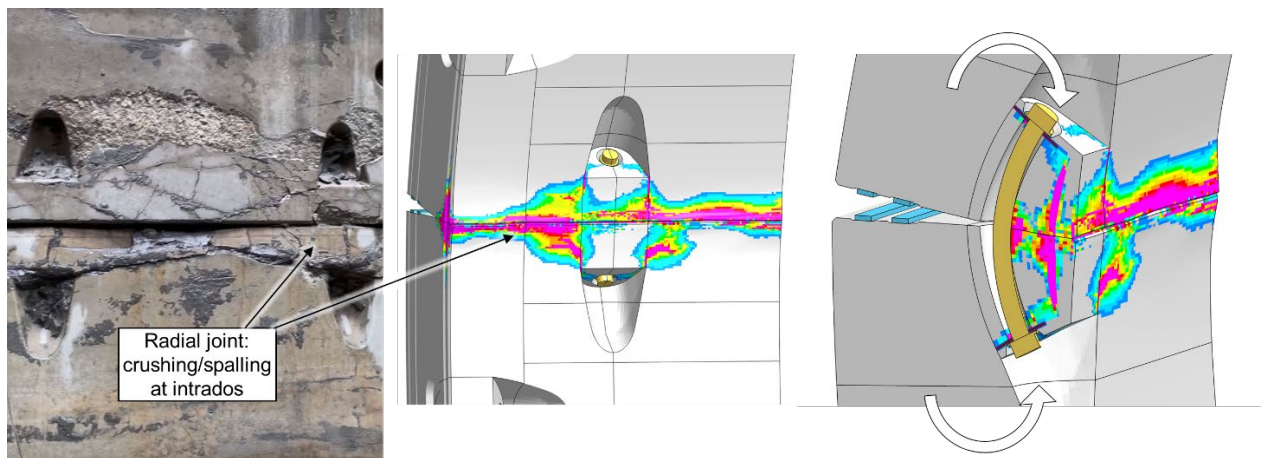


Fig.19: Simulation of extrados-opening rotation of radial joint compared with excavated segments

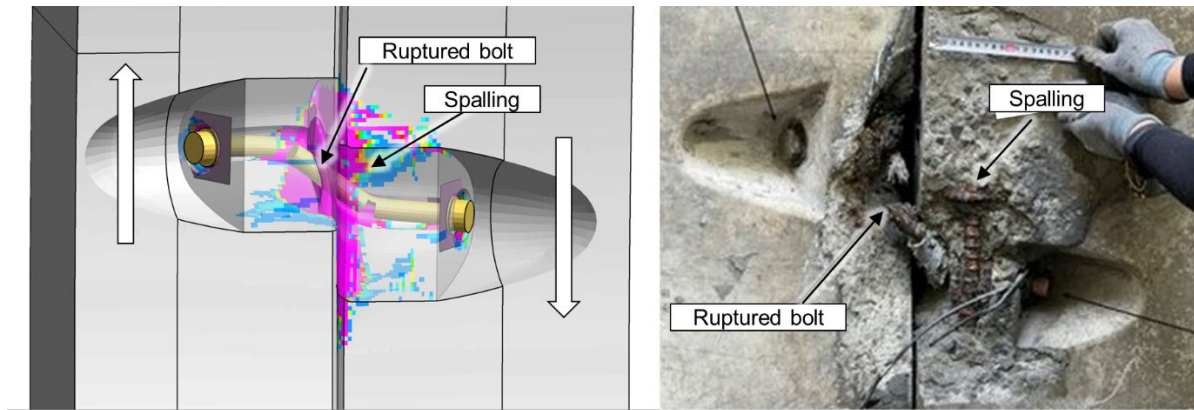


Fig.20: Simulation of circumferential shear of circle joint compared with excavated segments

5.3 Bearing strength of SFRC tunnel segments

Tunnel segments are sometimes designed with convex joint faces to reduce sensitivity to small misalignments during construction. Compressive load on the joint face is then concentrated over a small contact area. Tensile “bursting stress” develops parallel to the loaded surface at a small distance below the surface, leading to the possibility of splitting of the segment. Resistance to splitting under the maximum compressive load is one of the major considerations of segment design, and is often verified by full-scale testing. A series of such tests on SFRC segments has been modelled in LS-DYNA using MAT_084 (see Fig.21). The steel fibres resist widening of cracks, leading to a substantial margin between the load at which thin cracks are first observed versus the load at which failure occurs. Comparisons between the LS-DYNA model versus experimental results are shown in Table 1.

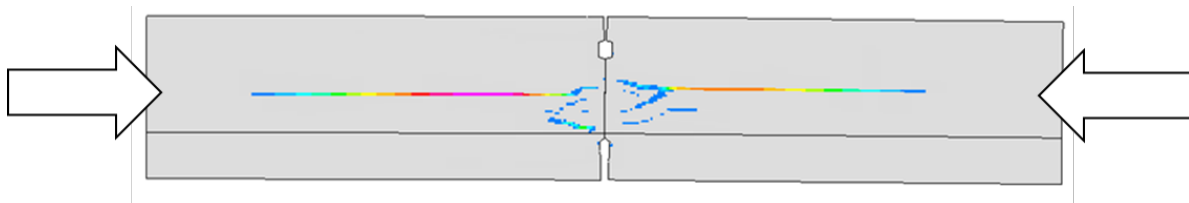


Fig.21: LS-DYNA simulation of SFRC tunnel segment compression test showing splitting failure. Loading direction shown by arrows.

	First crack	Ultimate Load
Test 1	0.45	1.01
Test 2	0.50	0.98
Test 3	0.46	1.01
FE Model	0.43	1.03

Table 1: SFRC tunnel segment test, forces non-dimensionalised to average experimental ultimate load

6 Summary

A series of features have been added to *MAT_WINFRITH_CONCRETE (*MAT_084), accessed by setting the input parameter RATE to 8 in versions of LS-DYNA starting from R15. These include confinement-dependent strain-softening response in compression, and improved cracking algorithm in tension with extensions for SFRC and modelling of aggregate interlock. The model is capable of realistic responses in simulations of material characterization tests such as cylinder and cube compression, splitting, shear, and notched beam tests. Examples have been given of its application to segmented concrete tunnel linings, but the material model is also suitable for modelling other types of concrete structures under static (or quasi-static) loading conditions. Detailed comparisons with other LS-DYNA material models for concrete (such as MAT_72R3 or CSCM) would be a useful topic for future investigations.

7 Acknowledgment

The authors wish to thank SK ecoplant co. ltd. for permission to include the photos and other project-related material in Section 5.2.

8 References

- [1] Broadhouse, B.J., "The Winfrith Concrete Model in LS-DYNA3D", Report SPD/D(95)363, AEA Technology, U.K., 1995.
- [2] Broadhouse, B.J. & Neilson, A.J., "Modelling Reinforced Concrete Structures in DYNA3D", Report AEEW-M 2465, United Kingdom Atomic Energy Authority, Winfrith, 1987.
- [3] Ottosen N.S., "A failure criterion for concrete". Journal of the Engineering Mechanics Division 103(4):527-35, 1977.
- [4] Taerwe L, Matthys S., "Fib model code for concrete structures", CEB-FIP, 2010.
- [5] Vecchio, F.J. & Collins, M.P., "The Modified Compression-Field Theory for Reinforced Concrete Elements Subjected to Shear", ACI J 83(2) (1986) pp219-231, 1986.
- [6] Montoya, E., Vecchio, F. J. & Sheikh, S. A., "Compression Field Modeling of Confined Concrete: Constitutive Models", Journal of Materials in Civil Engineering 18(4), 510-517, 2006.
- [7] Mander J.B., Priestley M.J. & Park R. "Theoretical stress-strain model for confined concrete". Journal of structural engineering 114(8) pp1804-26, 1988.
- [8] EN 12390-1:2012, "Testing hardened concrete. Part 1: Shape, dimensions and other requirements for specimens and moulds".
- [9] EN 12390-6:2009, "Testing hardened concrete. Part 6: Tensile splitting strength of test specimens".
- [10] EN 1992-1-1:2004+A1:2014, "Eurocode 2: Design of Concrete Structures – Part 1-1: General rules and rules for buildings".
- [11] Wong, R.C.K., Ma, S.K.Y., Wong, R.H.C. & Chau, K.T., "Shear strength of components of concrete under direct shearing". Cement and Concrete Research, 37(8), pp.1248-1256, 2007.
- [12] EN 14651:2005+A1:2007, "Test method for metallic fibre concrete. Measuring the flexural tensile strength (limit of proportionality (LOP), residual)".
- [13] AASHTO LRFD Bridge Design Specifications, 9th Edition, American Association of State Highway and Transportation Officials, 2020.